


Cite this: *Catal. Sci. Technol.*, 2022,  
12, 6838

# Effect of SO<sub>2</sub> poisoning on undoped and doped Mn-based catalysts for selective catalytic reduction of NO<sub>x</sub>

Javier Ruiz-Martínez, <sup>\*,a</sup> Lieven E. Gevers,<sup>a</sup> Linga R. Enakonda,<sup>a</sup>  
Ameen Shahid<sup>a</sup> and Fei Wen<sup>b</sup>

In this work, the poisoning effect of SO<sub>2</sub> was investigated in binary MnTi and ternary MnCeTi mixed oxides for the NH<sub>3</sub>-SCR reaction under conditions relevant for mobile applications. For the binary MnTi sample, catalytic activity increases up to 250 °C, and then drops due to the oxidation of ammonia to NO<sub>x</sub>. The addition of Ce decreases the catalytic activity at 150 °C but widens the optimal operational temperature and reaches high conversion at 350 °C. Upon performing activity test with 100 ppm of SO<sub>2</sub> in the gas stream, catalytic activity drastically decreases in all catalyst samples. The shape of the deactivation curve and SO<sub>2</sub> concentrations at the outlet of the reactor suggest a strong adsorption and poisoning of SO<sub>2</sub> on all the catalysts. Although samples containing large amounts of Ce display a better SO<sub>2</sub> tolerance, this is insufficient to be considered for practical applications. Deactivated samples were investigated by a wide range of characterization tools. N<sub>2</sub> physisorption measurements reveal a drop in the surface area that could partially explain catalyst deactivation. TGA reveals the absence of (NH<sub>4</sub>)<sub>2</sub>SO<sub>4</sub> on the deactivated samples and suggests the formation of Mn and Ce sulfates on the catalyst surface. XPS results confirm the formation of MnSO<sub>4</sub> and also show a decrease in the Mn and Ce oxidation states. Analysis of the redox function by catalytic NO oxidation and H<sub>2</sub>-TPR experiments shows a strong loss of redox function upon SO<sub>2</sub> deactivation, which could explain the decrease of NH<sub>3</sub>-SCR catalytic activity. Upon unraveling the effect and cause of deactivation, a doping study was performed. As in the binary MnTi and ternary MnCeTi, catalytic activity strongly decreases upon the introduction of SO<sub>2</sub> in the gas stream. None of the dopants investigated was able to suppress SO<sub>2</sub> deactivation, which suggest that other dopants or strategies should be pursued to commercialize Mn-based catalysts for low-temperature applications.

Received 11th July 2022,  
Accepted 28th September 2022

DOI: 10.1039/d2cy01151d

rsc.li/catalysis

## 1. Introduction

Selective catalytic reduction (SCR) with ammonia is one of the most promising technologies to abate nitric oxides (NO<sub>x</sub>, which includes NO and NO<sub>2</sub>) under lean-burning conditions encountered in mobile lean-burn engines and stationary applications.<sup>1–3</sup> Currently, there is a search for more efficient SCR catalysts motivated by the ever-increasing demand of stringent global legislation for improving air quality.<sup>4</sup> V<sub>2</sub>O<sub>5</sub>-WO<sub>3</sub>/TiO<sub>2</sub> catalysts provide high NO<sub>x</sub> removal efficiency (over 90%) at high gas-hourly space velocities (60 000–90 000 h<sup>-1</sup>)

and between 250 and 400 °C.<sup>5–8</sup> Unfortunately, the emission of toxic V oxides during operation has restricted such catalysts for mobile applications. Cu-CHA zeolites (Cu-SSZ-13 and Cu-SAPO-34) have been revolutionary in SCR applications due to their high activity and broader operational temperature (200–450 °C).<sup>9–11</sup> Still, great advances in engine technology have brought more efficient combustion engines and consequently lower exhaust temperatures, which makes NO<sub>x</sub> more refractory to abate, even for Cu-zeolites. Due to this situation, low-temperature (below 200 °C) catalysts are required. In this field, Mn-based catalysts have exhibited optimal NH<sub>3</sub>-SCR activity due to their strong redox functionality. Typically, Mn-oxide catalysts contain other metal oxides that serve as supports and modulate their catalytic properties. Although Mn-oxide catalysts have shown their superior performance at low-temperature NH<sub>3</sub>-SCR, they are not commercialized in automotive applications. One of the main reasons is their strong intolerance to SO<sub>2</sub>,<sup>12–15</sup> which is due to the combustion of sulfur contaminants in

<sup>a</sup> King Abdullah University of Science and Technology, KAUST Catalysis Center, Catalysis Nanomaterials and Spectroscopy (CNS), Thuwal 23955, Saudi Arabia.  
E-mail: javier.ruizmartinez@kaust.edu.sa

<sup>b</sup> Umicore AG & Co. KG, Rodenbach Chaussee 4, 63457 Hanau-Wolfgang, Germany

† Electronic supplementary information (ESI) available. See DOI: <https://doi.org/10.1039/d2cy01151d>



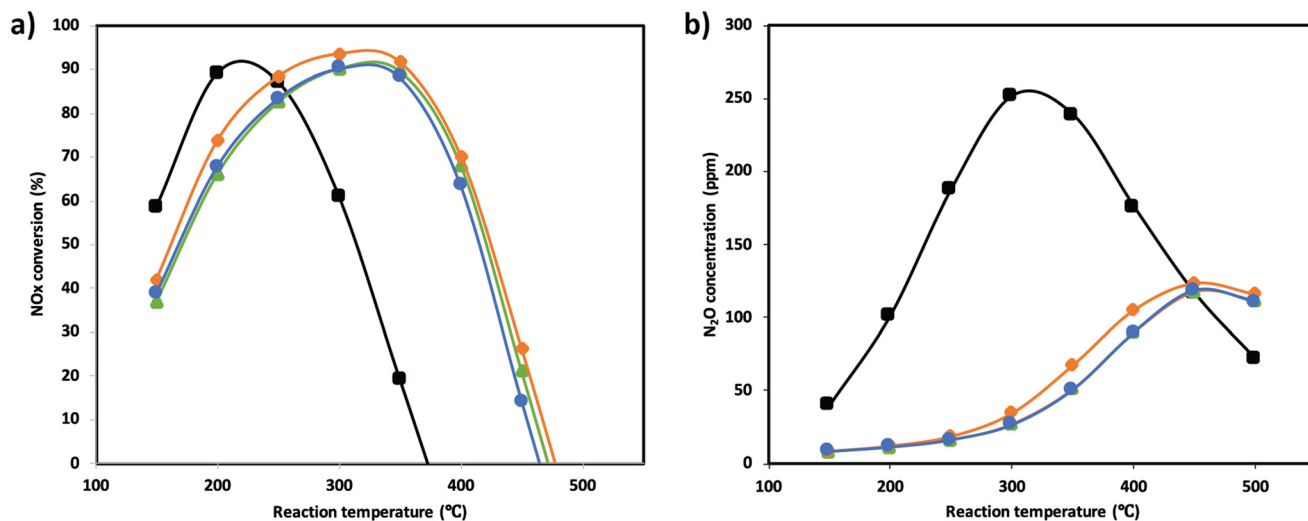


Fig. 1 NO<sub>x</sub> conversion (a) and N<sub>2</sub>O concentration (b) as a function of the reaction temperature for Mn<sub>0.35</sub>Ce<sub>0.00</sub>Ti<sub>0.65</sub> (black), Mn<sub>0.37</sub>Ce<sub>0.04</sub>Ti<sub>0.59</sub> (orange), Mn<sub>0.33</sub>Ce<sub>0.07</sub>Ti<sub>0.60</sub> (green), and Mn<sub>0.30</sub>Ce<sub>0.19</sub>Ti<sub>0.51</sub> (blue).

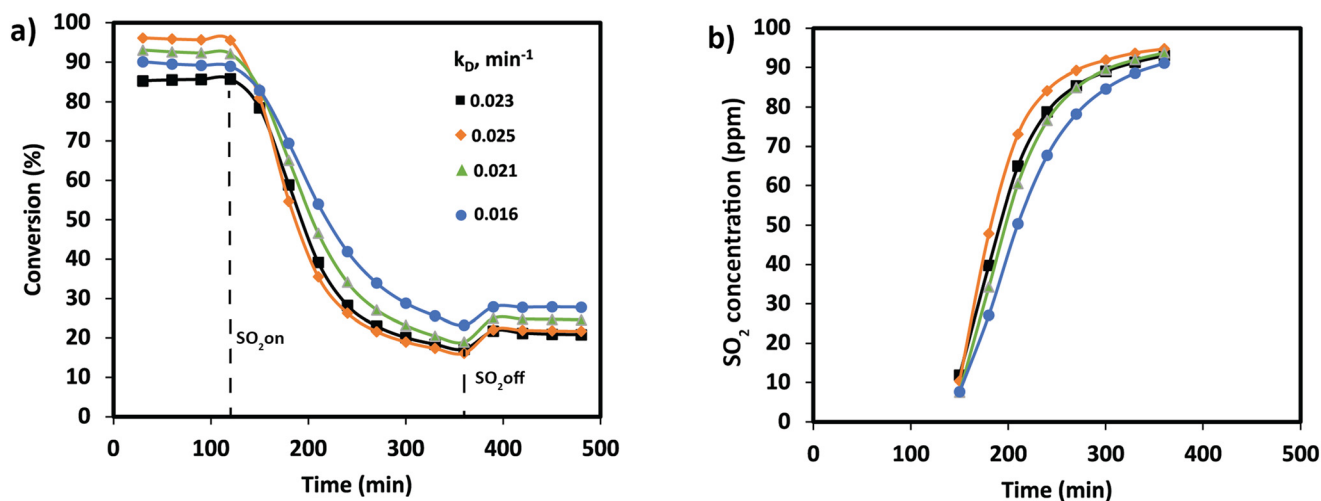


Fig. 2 a) Conversion plots and deactivation constants and b) SO<sub>2</sub> concentration at the outlet during the deactivation experiments performed at 250 °C for Mn<sub>0.35</sub>Ce<sub>0.00</sub>Ti<sub>0.65</sub> (black), Mn<sub>0.37</sub>Ce<sub>0.04</sub>Ti<sub>0.59</sub> (orange), Mn<sub>0.33</sub>Ce<sub>0.07</sub>Ti<sub>0.60</sub> (green), and Mn<sub>0.30</sub>Ce<sub>0.19</sub>Ti<sub>0.51</sub> (blue).

fuels and lubricants. Although the SO<sub>2</sub> concentration could be as low as a few ppm, those are sufficient to effectively poison Mn-oxide catalyst's active sites.

Several studies have discussed the detrimental effect of SO<sub>2</sub> on Mn-based catalysts and the deactivation effect has been explained by two main reasons. The first one is due to the reaction of SO<sub>2</sub> and NH<sub>3</sub> and H<sub>2</sub>O to form (NH<sub>4</sub>)<sub>2</sub>SO<sub>4</sub> and NH<sub>4</sub>HSO<sub>4</sub>, which deposit on the catalyst surface and have a

high decomposition temperature (230 and 350 °C), respectively.<sup>16,17</sup> The second one is related to the formation of metal sulfates that might modify or deactivate the active sites. Blik *et al.* investigated the SO<sub>2</sub> deactivation of MnO<sub>x</sub>/Al<sub>2</sub>O<sub>3</sub> catalysts by IR spectroscopy and found that the formation of MnSO<sub>4</sub> is the main source of deactivation.<sup>18</sup> There are reports describing the regeneration of SO<sub>2</sub>-poisoned catalysts can be efficient by water washing.<sup>19</sup> Unfortunately, this approach is unfeasible for *in situ* catalyst regeneration in a real mobile application. To solve this deactivation process, catalyst formulations were modified with Fe,<sup>20–23</sup> Co,<sup>24,25</sup> Ni,<sup>26,27</sup> W<sup>28</sup> and Sm<sup>29,30</sup> to improve their tolerance to SO<sub>2</sub> and H<sub>2</sub>O. For example, Wang *et al.* shown that Fe and Co co-doping reduces the adsorption of SO<sub>2</sub> on Mn–Ce/TiO<sub>2</sub> catalysts.<sup>23</sup> Sm-doped mixed oxide catalysts were shown to exhibit considerably enhanced catalytic activity and

Table 1 SO<sub>2</sub> uptake during deactivation experiments

Sample	SO <sub>2</sub> uptake (μmol g <sup>-1</sup> )	SO <sub>2</sub> uptake (μmol m <sup>-2</sup> )
Mn <sub>0.35</sub> Ce <sub>0.00</sub> Ti <sub>0.65</sub>	139	1.2
Mn <sub>0.37</sub> Ce <sub>0.04</sub> Ti <sub>0.59</sub>	119	0.6
Mn <sub>0.33</sub> Ce <sub>0.07</sub> Ti <sub>0.60</sub>	165	0.7
Mn <sub>0.30</sub> Ce <sub>0.19</sub> Ti <sub>0.51</sub>	182	0.7



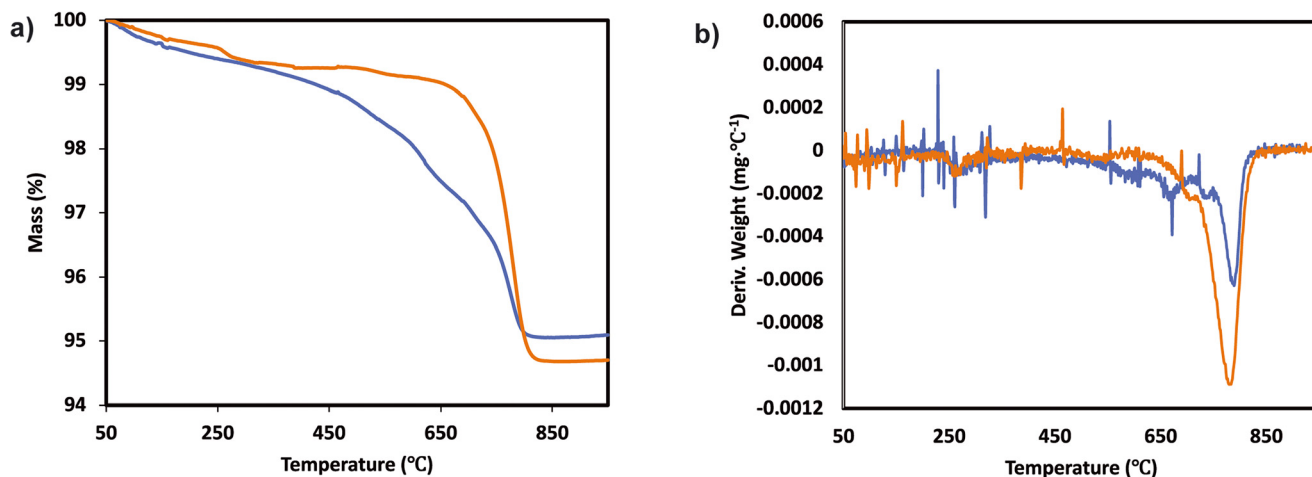


Fig. 3 a) TGA analysis and b) derivative thermogravimetric curves of the  $\text{Mn}_{0.35}\text{Ce}_{0.00}\text{Ti}_{0.65}$  sample after normal  $\text{NH}_3$ -SCR reaction (blue) and  $\text{NH}_3$ -SCR reaction with  $\text{SO}_2$  (yellow).

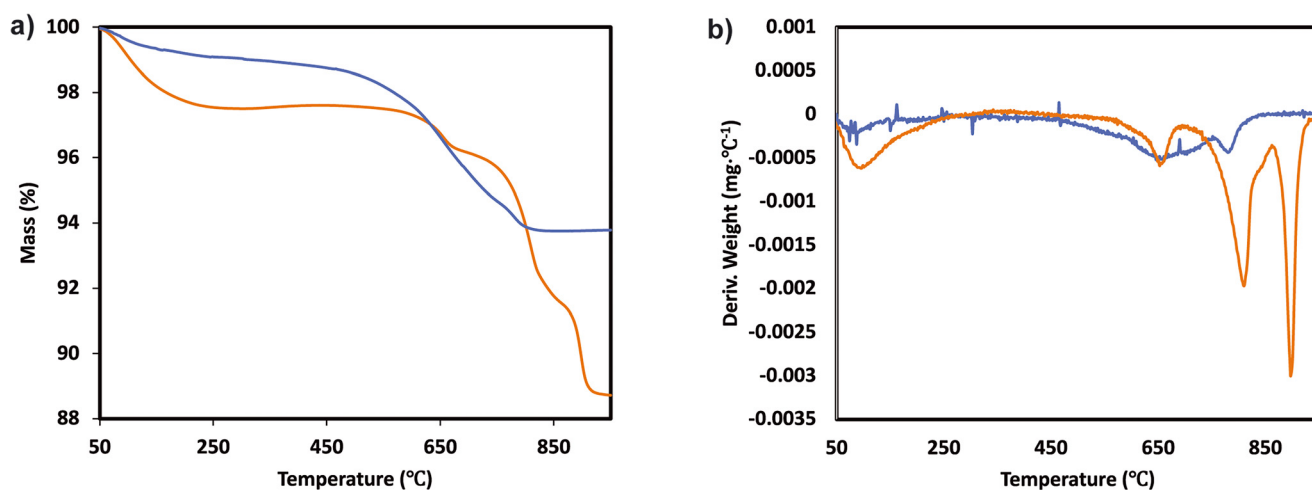


Fig. 4 a) TGA analysis and b) derivative thermogravimetric curves of the  $\text{Mn}_{0.37}\text{Ce}_{0.04}\text{Ti}_{0.59}$  ternary system after normal  $\text{NH}_3$ -SCR reaction (blue) and  $\text{NH}_3$ -SCR reaction with  $\text{SO}_2$  (yellow).

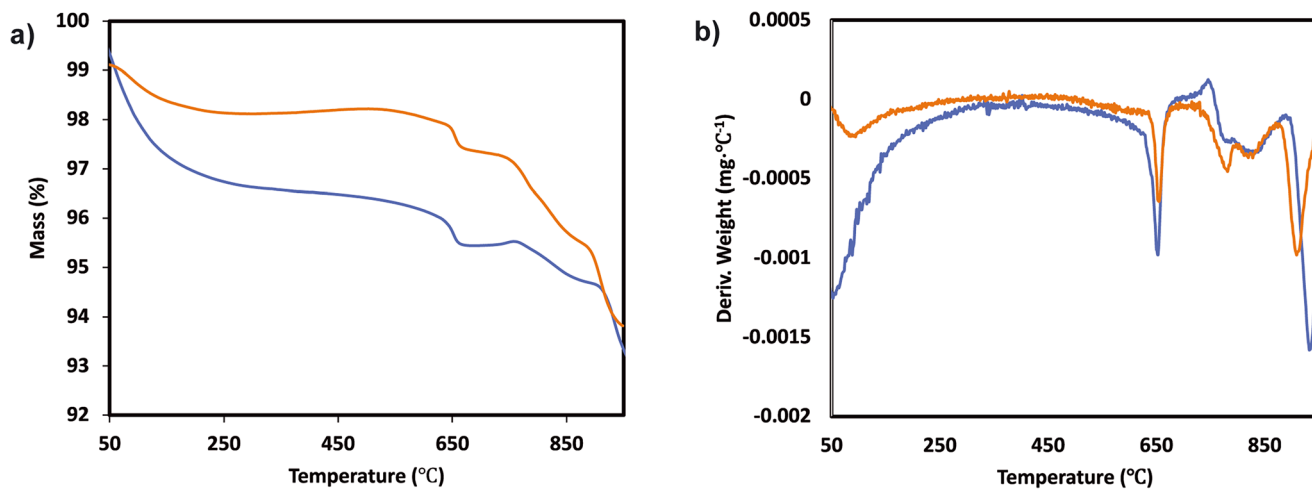


Fig. 5 a) TGA analysis and b) derivative thermogravimetric curves of the  $\text{Mn}_{0.30}\text{Ce}_{0.19}\text{Ti}_{0.51}$  ternary system after normal  $\text{NH}_3$ -SCR reaction (blue) and  $\text{NH}_3$ -SCR reaction with  $\text{SO}_2$  (yellow).



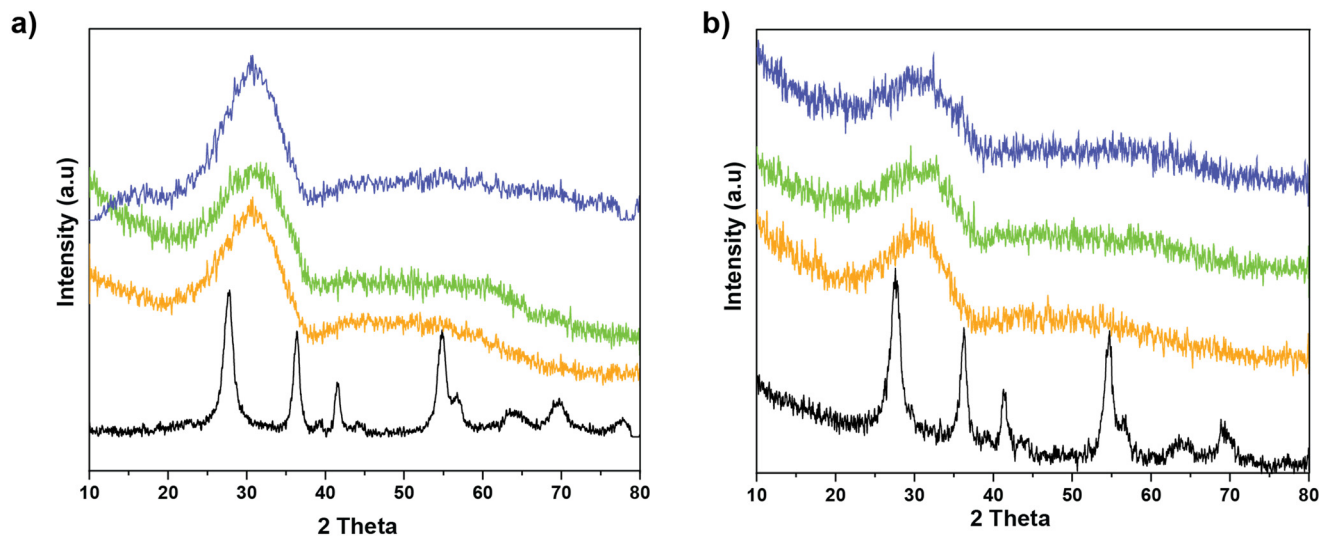


Fig. 6 X-ray diffraction patterns of the  $\text{Mn}_{0.35}\text{Ce}_{0.00}\text{Ti}_{0.65}$  (black),  $\text{Mn}_{0.37}\text{Ce}_{0.04}\text{Ti}_{0.59}$  (orange),  $\text{Mn}_{0.33}\text{Ce}_{0.07}\text{Ti}_{0.60}$  (green), and  $\text{Mn}_{0.30}\text{Ce}_{0.19}\text{Ti}_{0.51}$  (blue) samples: a) fresh and b) after  $\text{SO}_2$  deactivation.

$\text{SO}_2$  tolerance. Sun *et al.*<sup>29</sup> found that the electron transfer from  $\text{Sm}^{2+}$  to  $\text{Mn}^{4+}$  restrained the electron transfer from  $\text{SO}_2$  to  $\text{Mn}^{4+}$ , thereby suppressing the formation of  $\text{SO}_3$  and sulfate species. Meng *et al.*<sup>31</sup> found that a  $\text{SmO}_x\text{-MnO}_x$  catalyst had an ideal  $\text{SO}_2$  tolerance at low temperature, and they suggested that the incorporation of Sm could induce the formation of bulk-like sulfates on the Sm sites and weaken the influence of  $\text{SO}_2$  on the Mn sites. However, the origin of the effect of Sm doping into the catalysts on the  $\text{SO}_2$  tolerance is still unclear, and an in-depth study is still needed.

In this work, we aimed to understand the poisoning effect of  $\text{SO}_2$  on a MnTi binary mixed oxide. Then, the role of Ce in catalyst deactivation was investigated in MnCeTi tertiary mixed oxides with different amounts of Ce. For this purpose,  $\text{NH}_3\text{-SCR}$  reactions were performed by adding an amount of  $\text{SO}_2$  equivalent to the total amount of S that a catalyst will be exposed in the exhaust of a real internal combustion engine after 200 000 km. The activity recovery was assessed by a regeneration step under high temperature and  $\text{NH}_3\text{-SCR}$  conditions. These conditions were applied to simulate a theoretical regeneration in a real mobile application. After that, the catalysts were promoted by a wide range of metal dopants to evaluate the effect on poisoning and on catalyst regeneration.

## 2. Experimental

A series of individual, binary and ternary materials with different molar concentrations were prepared. Titanium(IV)

Table 2 Sulfur composition of the samples in the bulk and on the surface

Sample	Surface composition (mol%)	Bulk composition (mol%)
$\text{Mn}_{0.35}\text{Ce}_{0.00}\text{Ti}_{0.65}$	6.4	3
$\text{Mn}_{0.37}\text{Ce}_{0.04}\text{Ti}_{0.59}$	6.9	5.3
$\text{Mn}_{0.30}\text{Ce}_{0.19}\text{Ti}_{0.51}$	7.8	3.3

sulfate solution ( $\text{Ti}(\text{SO}_4)_2$ , Pfaltz & Bauer, 30% in  $\text{H}_2\text{SO}_4$ ), cerium(III) nitrate hexahydrate ( $\text{Ce}(\text{NO}_3)_3 \cdot 6\text{H}_2\text{O}$ , Sigma-Aldrich, 99.999% trace metals basis), manganese(II) nitrate hydrate ( $\text{Mn}(\text{NO}_3)_2 \cdot x\text{H}_2\text{O}$ , Sigma-Aldrich, 99.999% trace metals basis), and ammonium hydroxide ( $\text{NH}_4\text{OH}$ , Alfa Aesar, ACS grade, 28.0–30.0%) were used as received, without further purification. The binary MnTi and ternary MnCeTi were prepared by a controlled co-precipitation method described in our previous publication.<sup>32</sup> The method was designed to precipitate all metals at the same pH level to obtain a homogeneously well-mixed metal oxide system.

For the doping of the ternary MnCeTi catalysts, precipitation and impregnation methods were explored. In the precipitation method, a ternary MnCeTi was first suspended in an aqueous solution (50 mL). Then, 50 mL aqueous solution with the dopants were added slowly to the MnCeTi suspension, then the suspension was stirred for 30 min. After that, an aqueous ammonium hydroxide solution was added dropwise to the suspension under continuous stirring until a pH of 10.5 was reached. This was performed to precipitate all metal precursors on the catalyst surface. Afterwards, the suspension was stirred for another 1 h and then filtered. The solid product was washed with water 5–6 times, then dried in a hot air-oven overnight. For the impregnation method, 3 g of ternary MnCeTi sample were suspended in 50 mL of water. After 30 min of stirring, 50 mL of an aqueous solution of the dopant precursor were slowly added to the catalyst suspension. After stirring for 24 h, the suspension was evaporated and the solid was dried overnight. All catalysts were calcined at 500 °C for 6 h.

For the TG/DTA-MS analysis, 10–20 mg of sample was used. The samples were first kept at 30 °C for 30 min to stabilize the mass-loss signal. Then, the sample was heated with a ramp of 10 °C  $\text{min}^{-1}$  to 950 °C at 10 mL  $\text{min}^{-1}$  of air. The analysis of the gases was performed by mass



**Table 3** Surface composition and chemistry of Mn and Ce species measured by XPS

Sample	Surface composition (at%)		Manganese				Cerium	
	Mn	Ce	MnO <sub>2</sub>	Mn <sub>2</sub> O <sub>3</sub>	MnO	MnSO <sub>4</sub>	Ce(IV)	Ce(III)
Mn <sub>0.35</sub> Ce <sub>0.00</sub> Ti <sub>0.65</sub>	15.2	0.0	17.9	66.1	16.0	0.0	0.0	0.0
Mn <sub>0.35</sub> Ce <sub>0.00</sub> Ti <sub>0.65</sub> SO <sub>2</sub>	12.3	0.0	1.1	33.4	56.0	9.5	0.0	0.0
Mn <sub>0.37</sub> Ce <sub>0.04</sub> Ti <sub>0.59</sub>	23.4	2.4	12.3	75.8	11.9	0.0	70.7	29.3
Mn <sub>0.37</sub> Ce <sub>0.04</sub> Ti <sub>0.59</sub> SO <sub>2</sub>	18.2	2.7	19.6	18.8	53.6	8.0	36.3	63.7
Mn <sub>0.30</sub> Ce <sub>0.19</sub> Ti <sub>0.51</sub>	14.5	6.3	20.6	27.3	42.3	9.7	66.2	33.8
Mn <sub>0.30</sub> Ce <sub>0.19</sub> Ti <sub>0.51</sub> SO <sub>2</sub>	10.5	6.0	18.9	17.2	42.4	21.3	38.1	61.9

**Table 4** Textural properties of the samples

Sample	BET surface area (m <sup>2</sup> g <sup>-1</sup> )	Total pore volume (cm <sup>3</sup> g <sup>-1</sup> )	Pore size (nm)
Mn <sub>0.35</sub> Ce <sub>0.00</sub> Ti <sub>0.65</sub>	117	0.45	14.0
Mn <sub>0.37</sub> Ce <sub>0.04</sub> Ti <sub>0.59</sub>	200	0.53	9.5
Mn <sub>0.33</sub> Ce <sub>0.07</sub> Ti <sub>0.60</sub>	222	0.63	10.0
Mn <sub>0.30</sub> Ce <sub>0.19</sub> Ti <sub>0.51</sub>	243	0.86	12.5
Mn <sub>0.35</sub> Ce <sub>0.00</sub> Ti <sub>0.65</sub> SO <sub>2</sub>	90	0.36	20.4
Mn <sub>0.37</sub> Ce <sub>0.04</sub> Ti <sub>0.59</sub> SO <sub>2</sub>	142	0.51	13.1
Mn <sub>0.33</sub> Ce <sub>0.07</sub> Ti <sub>0.60</sub> SO <sub>2</sub>	159	0.49	11.6
Mn <sub>0.30</sub> Ce <sub>0.19</sub> Ti <sub>0.51</sub> SO <sub>2</sub>	147	0.44	11.2

spectrometry by following the signal from H<sub>2</sub>O ( $m/e = 18$ ), NO ( $m/e = 30$ ), N<sub>2</sub>O ( $m/e = 44$ ) and SO<sub>2</sub> ( $m/e = 48$ ).

X-ray diffraction patterns were obtained using a Bruker D8 Advance A25 diffractometer in the Bragg–Brentano geometry with a Cu K<sub>α,β</sub> radiation source operated at 40 kV and 40 mA. β radiation was filtered out with a Ni plate. The diffractograms were measured with a step size of 0.05° in the 2θ range of 10–80°.

Nitrogen adsorption and desorption isotherms of the samples were measured at 77 K using a Micromeritics ASAP-2420 surface area and porosity analyzer instrument. The samples were previously evacuated at 300 °C for 3 hours. Specific surface areas and pore size distribution were calculated according to the multi-point Brunauer–Emmett–Teller (BET) and Barrett–Joyner–Halenda (BJH) methods,

respectively. From the adsorption data, total pore volumes were estimated at  $P/P_0 = 0.99$ . The elemental compositions (Mn, Ce, Ti) of the samples were determined using an inductively coupled plasma spectrometer (Model 8900, Agilent Technologies). The samples were dissolved in HF and HCl.

H<sub>2</sub>-TPR experiments were performed on an Autochem 2950 instrument equipped with a thermal conductivity detector and a dry ice/isopropanol cold trap (−78 °C) to remove H<sub>2</sub>O generated during the reduction. All catalysts (100 mg) were pretreated in a U-shaped quartz tubular microreactor in a flow of Ar at 250 °C for 2 h to yield a clean surface, and then cooled down to 40 °C temperature. Then, the temperature was raised from 40 to 1000 °C at a rate of 10 °C min<sup>−1</sup> under a flow of 10 vol% H<sub>2</sub> (90 vol% Ar).

Temperature-programmed desorption of ammonia (NH<sub>3</sub>-TPD) was used to determine the acidity of the fresh samples and samples deactivated by SO<sub>2</sub>. The experiments were performed in a fixed bed quartz tube reactor. Prior to the measurement, the samples were first pretreated at 500 °C under a N<sub>2</sub> flow. The reactor was cooled down at 100 °C and the samples were saturated with 1050 ppm NH<sub>3</sub> for 30 min. The samples were flushed with N<sub>2</sub> for 30 min at room temperature, and then the temperature was increased to 500 °C at a rate of 10 K min<sup>−1</sup>. The outlet gas composition (NH<sub>3</sub>, NO, NO<sub>2</sub>, N<sub>2</sub>O) was monitored by using a MultiGas™ 2030 FTIR continuous gas analyzer.

For the XPS study, a Kratos Axis Ultra X-ray photoelectron spectrometer equipped with a monochromatic Al K<sub>α</sub> source was used to determine the surface composition and chemical states of the samples. The C 1s signal for adventitious carbon (284.8 eV) was used to calibrate the sample energy. The chemical states of manganese and cerium in the catalysts

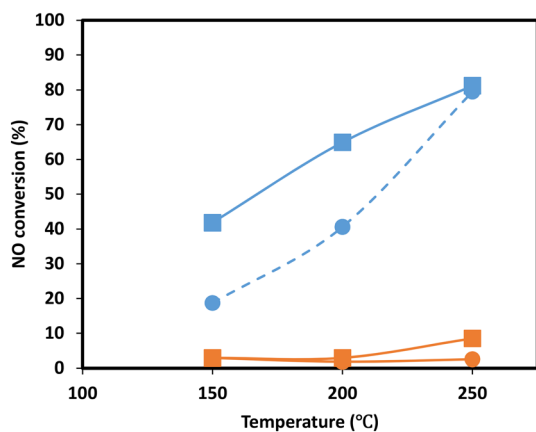


**Fig. 7** NO oxidation experiments of Mn<sub>0.37</sub>Ce<sub>0.04</sub>Ti<sub>0.59</sub> under dry (square) and wet (circle) conditions for the fresh sample (blue) and sample upon SO<sub>2</sub> deactivation (orange).



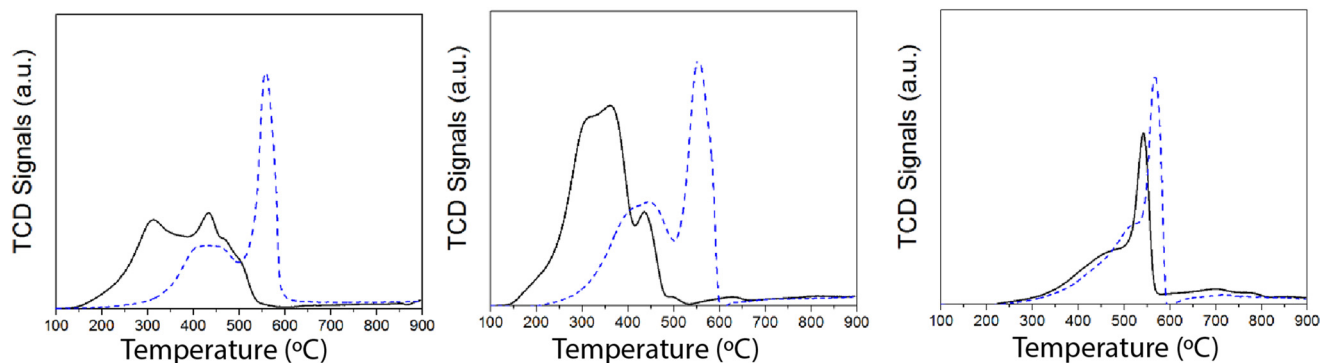


Fig. 8  $H_2$ -TPR results of S15, S24 and S28: fresh (solid line) and  $SO_2$  deactivated (dashed line).

Table 5  $NH_3$ -SCR catalytic performance of sample  $Mn_{0.37}Ce_{0.04}Ti_{0.59}$  and doped samples via precipitation (ppt) and impregnation (imp) methods

Sample	Conversion before deactivation (%)		Conversion after $SO_2$ deactivation (%)	Conversion after $SO_2$ regeneration (%)	
	150 °C	250 °C	250 °C	150 °C	250 °C
$Mn_{0.37}Ce_{0.04}Ti_{0.59}$	47	95	48	4	28
1% Sm/ $Mn_{0.37}Ce_{0.04}Ti_{0.59}$ (ppt)	53	98	35	2	24
1% V/ $Mn_{0.37}Ce_{0.04}Ti_{0.59}$ (ppt)	57	98	38	6	58
1% La/ $Mn_{0.37}Ce_{0.04}Ti_{0.59}$ (ppt)	68	98	47	6	34
1% Mo/ $Mn_{0.37}Ce_{0.04}Ti_{0.59}$ (imp)	45	96	28	4	52
1 wt% Eu/ $Mn_{0.37}Ce_{0.04}Ti_{0.59}$ (imp)	72	95	25	3	34

were determined by peak modeling in CasaXPS software. To model the Mn 2p<sub>3/2</sub> peaks of the catalysts, pure MnO, Mn<sub>2</sub>O<sub>3</sub>, and MnO<sub>2</sub> samples were used as references. Manganese(IV) oxide (99.997% – metals basis) was acquired from Alfa Aesar (Fisher US), manganese(III) oxide (99.9% – trace metals basis) was acquired from Sigma Aldrich, and manganese(II) oxide (99.99% – trace metal basis) was acquired from Acros Organics (VWR). The fitting parameter data (FWHM and peak positions) obtained from the peak modeling of the standard samples were used for the calculation of the chemical state of manganese in our catalysts. More details about the fitting procedure and measurements can be obtained in our previous publication.<sup>32</sup>

The catalytic activity measurements of the catalysts in the  $NH_3$ -SCR reaction were carried out in a fixed bed quartz tube reactor loaded with 0.5 ml of sample (PID Eng&Tech). Before loading, the catalysts were pressed into pellets, crushed and sieved to obtain a fraction between 500 and 710  $\mu m$ . The application-relevant catalyst particle size, space velocity and gas composition were applied. The inlet  $NO_x$  composition contained no  $NO_2$  to avoid higher conversions coming from the “fast SCR” mechanism when this gas is present. The total flow rate was maintained at 1000 ml  $min^{-1}$ , and the reaction condition corresponds to a GHSV of 120 000  $hr^{-1}$ . The flow rate of gases was controlled using Bronkhorst mass flow controllers. A controlled evaporation and mixing (CEM) system from Bronkhorst was used for evaporation to achieve the target steam content in the gas feed before entering the reactor. The inlet gas stream contained 450 ppm  $NO$ , 500 ppm  $NH_3$ , 5%  $O_2$ , 5%  $H_2O$  and  $N_2$  balance. A MultiGas™

2030 FTIR continuous gas analyzer was used to analyze the inlet and outlet gas compositions ( $NO$ ,  $NO_2$ ,  $NH_3$ ,  $N_2O$ ). The catalytic tests were performed in the temperature range of 150–500 °C (with an interval of 50 °C) at ambient pressure.  $NO$  conversion and  $N_2O$  selectivities were calculated under steady-state conditions. The SCR activity ( $NO$  conversion) and  $N_2$  selectivity are calculated as follows:

$$NO \text{ conversion (\%)} = \frac{[NO]_{in} - [NO]_{out}}{[NO]_{in}} \times 100 \quad (1)$$

$$N_2O \text{ selectivity (\%)} = \frac{2[N_2O]_{out}}{[NO_x]_{in} + [NH_3]_{in} - [NO_x]_{out} - [NH_3]_{out}} \times 100 \quad (2)$$

where  $[NH_3]_{in}$ ,  $[NO_x]_{in}$ ,  $[NH_3]_{out}$ ,  $[NO_x]_{out}$ , and  $[N_2O]_{out}$  are the concentrations of  $NH_3$  and  $NO_x$  (including  $NO$  and  $NO_2$ ) at the inlet and those at the outlet.

The  $NO$  oxidation reaction was performed in the same fashion as the  $NH_3$ -SCR. In this case, 250 ppm of  $NO$  and 5%  $O_2$  were fed to the reactor and balanced with  $N_2$ . In the experiments under wet conditions, 5% of vapor  $H_2O$  was included in the inlet gas stream.

### 3. Results

#### Activity measurements

$NO_x$  conversion of the MnTi binary and MnCeTi ternary mixed oxides as a function of the reaction temperature is presented in Fig. 1. The data at 150 °C were determined to be free of external and internal mass transport limitations (more



details in the ESI†). In general, conversion increases until reaching a maximum, and then decreases with the reaction temperature.  $\text{NH}_3$  conversion (ESI† Fig. S1) follows the same trend as  $\text{NO}_x$  conversion, but monotonically increases when the conversion drops. This mismatch in conversions is related to the undesired combustion of ammonia, which leads to the formation of additional  $\text{NO}_x$  in the gas stream. The binary MnTi catalyst is more active at low temperatures but lacks  $\text{N}_2$  selectivity, showing a high concentration of  $\text{N}_2\text{O}$  at the outlet (see Fig. 1b). The addition of Ce has several effects on catalytic performance. First, low-temperature activity decreases suggesting that Mn species are less active due to the interaction with Ce, as we previously reported.<sup>32</sup> Second, the addition of Ce widens the operational window, as was also reported previously,<sup>3</sup> and finally promotes  $\text{N}_2$  selectivity.

In order to understand the effect of  $\text{SO}_2$  poisoning, experiments were performed where  $\text{NO}_x$  conversion was measured before and during  $\text{SO}_2$  poisoning under  $\text{NH}_3$ -SCR conditions. Fig. 2 shows the  $\text{NH}_3$ -SCR conversion at 250 °C before and during  $\text{SO}_2$  deactivation. When 100 ppm  $\text{SO}_2$  is introduced in the stream, the conversion of all samples drastically decreased from  $\approx 90\%$  to  $\approx 20\%$  in 4 hours. Interestingly, the sample with the largest amount of Ce ( $\text{Mn}_{0.30}\text{Ce}_{0.19}\text{Ti}_{0.51}$ ) displays a better sulfur tolerance. The S-type shape of the deactivation curves suggest that  $\text{SO}_2$  is adsorbing strongly on the catalyst surface and deactivating the catalyst bed from the inlet to the outlet. Deactivation rates were consistently compared using second-order deactivation kinetics by applying the equation  $da/dt = -k_D \cdot a^2$  where  $a$  is the normalized  $\text{NO}_x$  activity. Deactivation rate constants, in Fig. 2a, are more pronounced for the binary MnTi catalyst and the samples with a small amount of Ce ( $\text{Mn}_{0.37}\text{Ce}_{0.04}\text{Ti}_{0.59}$ ). Then, deactivation constants drop when the amount of Ce increases, suggesting a lessening of deactivation with increasing Ce content. After removal of  $\text{SO}_2$  from the feed gas,  $\text{NO}_x$  conversion is marginally recovered indicating that  $\text{SO}_2$  deactivation is mostly irreversible.

$\text{SO}_2$  uptakes were calculated by monitoring the  $\text{SO}_2$  concentration at the reactor outlet in Fig. 2b. Clearly, the drop in  $\text{NO}_x$  conversion is strongly related to the  $\text{SO}_2$  uptake. The results show that all catalysts are adsorbing all  $\text{SO}_2$  at the first stage of the experiment. Then, the  $\text{SO}_2$  concentration is monotonically increasing until almost reaching the inlet concentration.  $\text{SO}_2$  uptakes, in Table 1, show an increase in the uptake for MnCeTi ternary catalysts with higher Ce loading. To rule out the effect of the surface area on the  $\text{SO}_2$  uptake, a surface normalization was applied. After such normalization, the results show a nearly constant  $\text{SO}_2$  adsorption in the MnCeTi ternary systems and therefore an independency from the amount of Ce. In the case of the binary MnTi, the  $\text{SO}_2$  uptake normalized by the surface area shows a twofold increase with respect to the Ce-containing samples. Our previous study showed that the surface of the binary MnTi samples is enriched with Mn,<sup>32</sup> which would suggest that sulfur prefers Mn to either Ti or Ce.

In order to understand if there are sulfates formed and their chemistry, thermogravimetric analysis (TGA) was performed with the samples before and after  $\text{SO}_2$  deactivation. The chemistry of the sulfate species was inferred by comparing the results with the TGA analysis results of pure  $(\text{NH}_4)_2\text{SO}_4$ ,  $\text{TiOSO}_4$ ,  $\text{MnSO}_4$ , and  $\text{Ce}(\text{SO}_4)_2$ . These results are included in the ESI† Fig. S2. The MnTi binary sample, in Fig. 3, shows a continuous decrease in mass loss after the normal  $\text{NH}_3$ -SCR reaction, which could be related to the removal of species adsorbed after the reaction. In the  $\text{NH}_3$ -SCR reaction with  $\text{SO}_2$ , there is a lack of mass loss at around 400 °C for the  $\text{SO}_2$  deactivated sample, which indicates that  $(\text{NH}_4)_2\text{SO}_4$  is not present in the deactivated material. In contrast, there is a remarkable increase in the weight loss at around 780 °C, which is a temperature slightly lower than the decomposition temperature of  $\text{MnSO}_4$  (see ESI†). Combined mass spectrometry measurements (in ESI† Fig. S3a) show an evolution of  $\text{SO}_2$  coming out of the sample, suggesting the decomposition of a metal sulfate. We hypothesized that the weight loss is due to the decomposition of  $\text{MnSO}_4$  and the fact that the decomposition temperature is slightly lower than that of pure bulk sulfates could be due to the fact that the sulfates might be finely dispersed on the catalyst surface. The existence of  $\text{TiOSO}_4$  is discarded due to the lack of weight loss and  $\text{SO}_2$  evolution at the decomposition temperature of such species.

The TGA analysis of the ternary  $\text{Mn}_{0.37}\text{Ce}_{0.04}\text{Ti}_{0.59}$  and  $\text{Mn}_{0.30}\text{Ce}_{0.19}\text{Ti}_{0.51}$  samples is shown in Fig. 4 and 5. The samples without deactivation show a slight mass loss around 800 °C with an  $\text{SO}_2$  evolution, suggesting that there are some sulfates formed during the catalyst synthesis due to the use of  $\text{TiOSO}_4$  as a titanium precursor. All samples have also mass loss around 650 °C, which could be related to the decomposition of  $\text{TiOSO}_4$ . However, this cannot be confirmed as there is no evolution of  $\text{SO}_3$  in the mass spectrometer. Measuring  $\text{SO}_3$  is quite challenging due to its highly reactive nature. Upon  $\text{SO}_2$  deactivation, there are several decomposition events at around 800 °C, which could be ascribed to the formation of both Ce and Mn sulfates. The existence of sulfates is corroborated by the evolution of  $\text{SO}_2$  during the TGA experiments.

To understand the structural changes occurring upon  $\text{SO}_2$  deactivation, the crystalline structure of the samples before and after deactivation was investigated by X-ray diffraction (XRD). The results, in Fig. 6, show that the MnCe binary oxide show reflections of rutile  $\text{TiO}_2$ , with no appearance of  $\text{MnO}_x$  phases. In the case of the MnCeTi ternary systems, the diffraction patterns lack any reflection indicating the amorphous nature of the samples. After  $\text{SO}_2$  deactivation, the diffraction patterns resemble the fresh counterparts. The lack of additional crystalline phases indicates that the metal sulfates have an amorphous nature, most likely due to the formation of the sulfates solely on the catalyst surface.

To further investigate the location of the sulfur species on the catalysts, the bulk and surface composition of sulfur was investigated by ICP and XPS, respectively. Table 2 shows the



sulfur composition in mol%. Clearly, all the samples show a sulfur enrichment on the catalyst surface compared to the total bulk composition, in line with the hypothesis that sulfur species are created more preferentially on the catalyst surface.

Experiments to understand the acidity of the samples upon SO<sub>2</sub> deactivation were performed by temperature-programmed desorption of ammonia (NH<sub>3</sub>-TPD). The temperature-programmed evolution of the binary Mn<sub>0.35</sub>-Ce<sub>0.00</sub>Ti<sub>0.65</sub> sample is plotted in ESI† Fig. S4. The amount of NH<sub>3</sub> desorbed is more than double after SO<sub>2</sub> deactivation (see ESI† Table S1), which reflect the formation of new acid sites. This insight has also been reported previously and indicates the acidic nature of the new sulfate species formed on the surface.<sup>33–35</sup> Additional information about the reactivity of oxygen species on the catalyst could be extracted from the evolution of N<sub>2</sub>O during NH<sub>3</sub>-TPD. Less N<sub>2</sub>O is formed at higher temperature after SO<sub>2</sub> deactivation, which points to the loss of active oxygen during deactivation.

To gain more insight into the effect of SO<sub>2</sub>, the chemistry of Mn and Ce was investigated by XPS. Oxidation states of Mn were rigorously fitted from a set of Gaussian–Lorentzian components per oxidation state, due to the multiplet splitting between the unpaired electrons in Mn 2+, 3+ and 4+. The set of components of the discrete oxidation states were obtained from measurements of pure MnSO<sub>4</sub>, MnO, Mn<sub>2</sub>O<sub>3</sub> and MnO<sub>2</sub> oxides and the results were compared with previously reported measurements.<sup>36</sup> The Mn 2p spectra of the reference samples and catalysts (fresh and SO<sub>2</sub> deactivated) are plotted in ESI† Fig. S5 and S6. Table 3 shows the surface composition and chemistry of Mn and Ce on selected samples. After SO<sub>2</sub> deactivation, Mn surface composition decreases whereas Ce remains nearly constant. The Mn (2p<sub>3/2</sub>) spectra show an overall change in the composition of the samples to more reduced Mn species. Although Mn<sub>2</sub>O<sub>3</sub> is dominant in the fresh samples, MnO is the most predominant species upon SO<sub>2</sub> deactivation. Additionally, a substantial amount of MnSO<sub>4</sub> is formed. Overall, around 60% of Mn<sup>4+</sup> and Mn<sup>3+</sup> gets reduced to Mn<sup>2+</sup>. Ce (3d) spectra show an increase in the concentration of Ce<sup>3+</sup> upon deactivation (see also ESI† Fig. S7), which could be explained by the oxidation of SO<sub>2</sub> to SO<sub>4</sub><sup>2-</sup> and the reduction of Ce<sup>4+</sup> to Ce<sup>3+</sup> with subsequent formation of sulfates.<sup>37</sup>

The N<sub>2</sub> physisorption results, in Table 4, show a surface area of the MnTi binary sample of 117 m<sup>2</sup> g<sup>-1</sup>. After the addition of Ce, there is an increase in the surface area and total pore volume, mostly related to the formation of an amorphous mixed-oxide phase. The samples after SO<sub>2</sub> deactivation show a drop in the specific surface area. In the case of the binary MnTi, 23% of the specific surface area is lost after deactivation. For the samples with Ce, the loss in the specific surface area increases with the amount of Ce (28, 29 and 40% for Mn<sub>0.33</sub>Ce<sub>0.07</sub>Ti<sub>0.60</sub>, Mn<sub>0.37</sub>Ce<sub>0.04</sub>Ti<sub>0.59</sub> and Mn<sub>0.30</sub>Ce<sub>0.19</sub>Ti<sub>0.51</sub>, respectively). Other authors have also observed a decrease in the surface area upon SO<sub>2</sub> deactivation on Mn-based catalysts,<sup>18,38,39</sup> mostly due to the

formation of surface sulphate species. Indeed, this loss in the surface area has a direct impact on catalyst deactivation. However, in our study, it can only explain catalyst deactivation to a limited extent. Therefore, this is not the main deactivation mechanism.

To gain more insight into the effect of SO<sub>2</sub> poisoning on catalytic performance, NO oxidation to NO<sub>2</sub> of the Mn<sub>0.37</sub>-Ce<sub>0.04</sub>Ti<sub>0.59</sub> ternary sample was performed before and after SO<sub>2</sub> deactivation. This is a model reaction to investigate the behavior of the catalyst redox function, which is strongly related to its NH<sub>3</sub>-SCR performance at low temperatures. Additionally, NO oxidation plays a key role in the fast SCR reaction, which is believed to be ten times faster than the standard reaction of NO with NH<sub>3</sub>.<sup>40,41</sup> As the NH<sub>3</sub>-SCR reaction is performed under the presence of H<sub>2</sub>O, the experiments were performed under dry and wet conditions. The results, in Fig. 7, show a clear drop in NO oxidation upon SO<sub>2</sub> deactivation in the range of temperatures investigated, suggesting that the redox function is drastically affected upon deactivation as it was also observed during the evolution of N<sub>2</sub>O in the NH<sub>3</sub>-TPD experiments. Several authors have also observed similar effects on CeO<sub>2</sub>-MnO<sub>x</sub><sup>42</sup> and MnO<sub>x</sub>/TiO<sub>2</sub> (ref. 43) catalysts and postulate that the reason is the formation of Mn sulfates.

Since the redox function seems to be strongly affected after SO<sub>2</sub> deactivation, additional insights were obtained by temperature-programmed reduction (TPR) experiments with H<sub>2</sub>. The H<sub>2</sub>-TPR results of the samples (fresh and after SO<sub>2</sub> deactivation) are shown in Fig. 8. Overall, we ascribe the reduction of the H<sub>2</sub> consumption peak at 200–450 °C to the reduction of Mn<sup>4+</sup> and Mn<sup>3+</sup> to Mn<sup>2+</sup>.<sup>44,45</sup> Upon SO<sub>2</sub> deactivation, there is a decrease in the H<sub>2</sub> consumed at those temperatures, most likely due to the overall reduction in the Mn oxidation state, as suggested by the XPS results. Additionally, H<sub>2</sub> consumption is shifted to higher temperatures, which could be rationalized as a consequence of the interaction of sulfate species with Mn. The strong H<sub>2</sub> consumption at 550–600 °C is related to the reduction of Mn and Ce sulfates.<sup>33,34,46</sup>

Overall, our results shows that catalyst deactivation is mainly due to the formation of metal sulfates, most likely Mn and Ce sulfates. These metal sulfates are decreasing the oxidation states of Mn and Ce, which have a strong impact on the redox function of such metals. Additionally, SO<sub>2</sub> deactivation decreases the catalysts' total specific surface area, but this is not the main deactivation mechanism.

In order to improve the catalytic properties of the samples upon deactivation, a thorough doping study was performed. Catalytic performances of the selected samples (fresh and upon SO<sub>2</sub>) and NH<sub>3</sub>-SCR regeneration at 500 °C for 30 min are shown in Table 5. On the selected metal-doped catalysts, relatively high NH<sub>3</sub>-SCR activities were obtained with the samples doped with Sm, V, La and Eu. Upon catalytic reaction with 100 ppm of SO<sub>2</sub>, the NH<sub>3</sub>-SCR activity was drastically decreased for both the undoped and doped samples. Therefore, the dopant seems to be ineffective in





avoiding catalyst deactivation under the investigated conditions.

To recover the catalyst activity, the samples were treated at 500 °C in 20% oxygen, as these conditions could be applied in a real exhaust of a combustion engine. The results show that in some samples, such conditions are even more detrimental, decreasing the catalyst activity upon SO<sub>2</sub> uptake. As exceptions, samples doped with V and Mo display an almost twofold increase in catalytic activity at 250 °C. As described in the literature, V and Mo are acidic metals and could inhibit the adsorption of SO<sub>2</sub> to some extent.<sup>47</sup> Unfortunately, activity at 150 °C is still poor, indicating that the addition of such metals is not sufficient to avoid the formation of Mn and Ce sulfates and therefore the loss of redox function. We hypothesized that the high activities at 250 °C are due to V and Mo themselves, which are active metals for NH<sub>3</sub>-SCR and are not that drastically affected by SO<sub>2</sub> deactivation. However, such metals are not sufficiently active at low temperatures. Our results are contradicting other previously reported data, for example summarized elsewhere,<sup>3</sup> where dopants improve sulfur tolerance. While reviewing those studies, one can see that most of them were performed at lower space velocities and/or in the absence of steam, which is not representative of a real application.

## 4. Conclusions

In this work, the poisoning effect of SO<sub>2</sub> was investigated in binary MnTi and ternary MnCeTi mixed oxides for the NH<sub>3</sub>-SCR reaction under conditions relevant for mobile applications. Upon performing activity test with 100 ppm of SO<sub>2</sub> in the gas stream, the catalytic activity drastically decreases in all catalyst samples. The shape of the deactivation curve and SO<sub>2</sub> concentrations out of the reactor suggest a strong adsorption and poisoning of SO<sub>2</sub> on all the catalysts. Although samples containing large amounts of Ce display a better SO<sub>2</sub> tolerance, this is insufficient to be considered for realistic practical applications. Spent samples were investigated by a wide range of characterization tools. N<sub>2</sub> physisorption measurements reveal a drop in the surface area that could partially explain catalyst deactivation. TGA reveals the absence of (NH<sub>4</sub>)<sub>2</sub>SO<sub>4</sub> on the deactivated samples and suggests the formation of Mn and Ce sulfates on the catalyst surface. XPS results confirm the formation of MnSO<sub>4</sub> and also show a decrease in the Mn and Ce oxidation states. Analysis of the redox function by catalytic NO oxidation and H<sub>2</sub>-TPR experiments shows a strong loss of redox function upon SO<sub>2</sub> deactivation, which could explain the decrease in NH<sub>3</sub>-SCR catalytic activity. Upon unraveling the effect and cause of deactivation, the catalysts were modified by doping with a wide range of metals. As in the binary MnTi and ternary MnCeTi, catalytic activity strongly decreases upon the introduction of SO<sub>2</sub> in the gas stream. None of the dopants investigated was able to suppress SO<sub>2</sub> deactivation nor regenerate catalyst activity at low temperatures, which suggest that other dopants or strategies should be pursued to

commercialize Mn-based catalysts for low-temperature applications.

## Conflicts of interest

The authors declare no competing interest.

## Acknowledgements

The authors thank the financial support from Umicore N.V. (award number RGC/3/3291-01). The research was supported by the resources and facilities provided by the King Abdullah University of Science and Technology. The authors also acknowledge the KAUST Imaging and Characterization Core Lab. Lutz Ruwisch (Umicore) is kindly acknowledged for fruitful discussion.

## References

- 1 J. L. Sorrels, Selective Catalytic Reduction. U.S. Environmental Protection Agency. <https://www.epa.gov/economic-and-cost-analysis-air-pollution-regulations/chapter-2-selective-catalytic-reduction>.
- 2 R. Zhang, N. Liu, Z. Lei and B. Chen, Selective Transformation of Various Nitrogen-Containing Exhaust Gases toward N<sub>2</sub> over Zeolite Catalysts, *Chem. Rev.*, 2016, **116**(6), 3658–3721.
- 3 L. Han, S. Cai, M. Gao, J. Y. Hasegawa, P. Wang, J. Zhang, L. Shi and D. Zhang, Selective Catalytic Reduction of NO<sub>x</sub> with NH<sub>3</sub> by Using Novel Catalysts: State of the Art and Future Prospects, *Chem. Rev.*, 2019, **119**(19), 10916–10976.
- 4 T. V. Johnson, Diesel emission control in review, *SAE Int. J. Fuels Lubr.*, 2009, **1**(1), 68–81.
- 5 J. Chen and R. Yang, Role of WO<sub>3</sub> in mixed V<sub>2</sub>O<sub>5</sub>-WO<sub>3</sub>/TiO<sub>2</sub> catalysts for selective catalytic reduction of nitric oxide with ammonia, *Appl. Catal., A*, 1992, **80**(1), 135–148.
- 6 T. Xu, X. Wu, Y. Gao, Q. Lin, J. Hu and D. Weng, Comparative study on sulfur poisoning of V<sub>2</sub>O<sub>5</sub>-Sb<sub>2</sub>O<sub>3</sub>/TiO<sub>2</sub> and V<sub>2</sub>O<sub>5</sub>-WO<sub>3</sub>/TiO<sub>2</sub> monolithic catalysts for low-temperature NH<sub>3</sub>-SCR, *Catal. Commun.*, 2017, **93**, 33–36.
- 7 X. Tian, Y. Xiao, P. Zhou, W. Zhang and X. Luo, Investigation on performance of V<sub>2</sub>O<sub>5</sub>-WO<sub>3</sub>-TiO<sub>2</sub>-cordierite catalyst modified with Cu, Mn and Ce for urea-SCR of NO, *Mater. Res. Innovations*, 2014, **18**(sup2), 202–206.
- 8 Z. Lian, Y. Li, W. Shan and H. He, Recent Progress on Improving Low-Temperature Activity of Vanadia-Based Catalysts for the Selective Catalytic Reduction of NO<sub>x</sub> with Ammonia, *Catalysts*, 2020, **10**(12), 1421.
- 9 D. W. Fickel and R. F. Lobo, Copper coordination in Cu-SSZ-13 and Cu-SSZ-16 investigated by variable-temperature XRD, *J. Phys. Chem. C*, 2010, **114**(3), 1633–1640.
- 10 J. Girard, G. Cavataio, R. Snow and C. Lambert, Combined Fe-Cu SCR systems with optimized ammonia to NO<sub>x</sub> ratio for diesel NO<sub>x</sub> control, *SAE Int. J. Fuels Lubr.*, 2009, **1**(1), 603–610.
- 11 J. H. Kwak, R. G. Tonkyn, D. H. Kim, J. Szanyi and C. H. Peden, Excellent activity and selectivity of Cu-SSZ-13 in the



- selective catalytic reduction of NO<sub>x</sub> with NH<sub>3</sub>, *J. Catal.*, 2010, **275**(2), 187–190.
- 12 B. Jiang, Y. Liu and Z. Wu, Low-temperature selective catalytic reduction of NO on MnO<sub>x</sub>/TiO<sub>2</sub> prepared by different methods, *J. Hazard. Mater.*, 2009, **162**(2), 1249–1254.
  - 13 S. Deng, T. Meng, B. Xu, F. Gao, Y. Ding, L. Yu and Y. Fan, Advanced MnO<sub>x</sub>/TiO<sub>2</sub> Catalyst with Preferentially Exposed Anatase {001} Facet for Low-Temperature SCR of NO, *ACS Catal.*, 2016, **6**(9), 5807–5815.
  - 14 E. Park, M. Kim, H. Jung, S. Chin and J. Jung, Effect of Sulfur on Mn/Ti Catalysts Prepared Using Chemical Vapor Condensation (CVC) for Low-Temperature NO Reduction, *ACS Catal.*, 2013, **3**(7), 1518–1525.
  - 15 S. Yu, Y. Lu, Y. Cao, J. Wang, B. Sun, F. Gao, C. Tang and L. Dong, Composite catalytic systems: A strategy for developing the low temperature NH<sub>3</sub>-SCR catalysts with satisfactory SO<sub>2</sub> and H<sub>2</sub>O tolerance, *Catal. Today*, 2019, **327**, 235–245.
  - 16 I. S. Nam, J. W. Eldridge and J. R. Kittrell, Deactivation of a vanadia-alumina catalyst for nitric oxide reduction by ammonia, *Ind. Eng. Chem. Prod. Res. Dev.*, 1986, **25**(2), 192–197.
  - 17 Q. Wang, J. Zhou, J. Zhang, H. Zhu, Y. Feng and J. Jin, Effect of ceria doping on catalytic activity and SO<sub>2</sub> resistance of MnO<sub>x</sub>/TiO<sub>2</sub> catalysts for selective catalytic reduction of NO with NH<sub>3</sub> at low temperature, *Aerosol Air Qual. Res.*, 2020, **20**, 477–488.
  - 18 W. Sjoerd Kijlstra, M. Biervliet, E. K. Poels and A. Blik, Deactivation by SO<sub>2</sub> of MnO<sub>x</sub>/Al<sub>2</sub>O<sub>3</sub> catalysts used for the selective catalytic reduction of NO with NH<sub>3</sub> at low temperatures, *Appl. Catal., B*, 1998, **16**(4), 327–337.
  - 19 Z. Sheng, Y. Hu, J. Xue, X. Wang and W. Liao, SO<sub>2</sub> poisoning and regeneration of Mn-Ce/TiO<sub>2</sub> catalyst for low temperature NO<sub>x</sub> reduction with NH<sub>3</sub>, *J. Rare Earths*, 2012, **30**(7), 676–682.
  - 20 S. Wu, X. Yao, L. Zhang, Y. Cao, W. Zou, L. Li, K. Ma, C. Tang, F. Gao and L. Dong, Improved low temperature NH<sub>3</sub>-SCR performance of FeMnTiO<sub>x</sub> mixed oxide with CTAB-assisted synthesis, *Chem. Commun.*, 2015, **51**(16), 3470–3473.
  - 21 F. Liu, H. He, Y. Ding and C. Zhang, Effect of manganese substitution on the structure and activity of iron titanate catalyst for the selective catalytic reduction of NO with NH<sub>3</sub>, *Appl. Catal., B*, 2009, **93**(1), 194–204.
  - 22 B. Q. Jiang, Z. B. Wu, Y. Liu, S. C. Lee and W. K. Ho, DRIFT Study of the SO<sub>2</sub> Effect on Low-Temperature SCR Reaction over Fe–Mn/TiO<sub>2</sub>, *J. Phys. Chem. C*, 2010, **114**(11), 4961–4965.
  - 23 F. Wang, B. Shen, S. Zhu and Z. Wang, Promotion of Fe and Co doped Mn-Ce/TiO<sub>2</sub> catalysts for low temperature NH<sub>3</sub>-SCR with SO<sub>2</sub> tolerance, *Fuel*, 2019, **249**, 54–60.
  - 24 H. Hu, S. Cai, H. Li, L. Huang, L. Shi and D. Zhang, Mechanistic Aspects of deNO<sub>x</sub> Processing over TiO<sub>2</sub> Supported Co–Mn Oxide Catalysts: Structure–Activity Relationships and In Situ DRIFTS Analysis, *ACS Catal.*, 2015, **5**(10), 6069–6077.
  - 25 L. Huang, X. Hu, S. Yuan, H. Li, T. Yan, L. Shi and D. Zhang, Photocatalytic preparation of nanostructured MnO<sub>2</sub>-(Co<sub>3</sub>O<sub>4</sub>)/TiO<sub>2</sub> hybrids: The formation mechanism and catalytic application in SCR deNO<sub>x</sub> reaction, *Appl. Catal., B*, 2017, **203**, 778–788.
  - 26 J. Liu, X. Li, R. Li, Q. Zhao, J. Ke, H. N. Xiao, L. Wang, S. Liu, M. O. Tadè and S. Wang, Facile synthesis of tube-shaped Mn-Ni-Ti solid solution and preferable Langmuir-Hinshelwood mechanism for selective catalytic reduction of NO<sub>x</sub> by NH<sub>3</sub>, *Appl. Catal., A*, 2018, **549**, 289–301.
  - 27 L. Chen, R. Li, Z. Li, F. Yuan, X. Niu and Y. Zhu, Effect of Ni doping in NixMn1-xTi10 (x = 0.1–0.5) on activity and SO<sub>2</sub> resistance for NH<sub>3</sub>-SCR of NO studied with in situ DRIFTS, *Catal. Sci. Technol.*, 2017, **7**(15), 3243–3257.
  - 28 X. Wang, X. Li, Q. Zhao, W. Sun, M. Tade and S. Liu, Improved activity of W-modified MnO<sub>x</sub>-TiO<sub>2</sub> catalysts for the selective catalytic reduction of NO with NH<sub>3</sub>, *Chem. Eng. J.*, 2016, **288**, 216–222.
  - 29 C. Sun, H. Liu, W. Chen, D. Chen, S. Yu, A. Liu, L. Dong and S. Feng, Insights into the Sm/Zr co-doping effects on N<sub>2</sub> selectivity and SO<sub>2</sub> resistance of a MnO<sub>x</sub>-TiO<sub>2</sub> catalyst for the NH<sub>3</sub>-SCR reaction, *Chem. Eng. J.*, 2018, **347**, 27–40.
  - 30 B. Wang, M. Wang, L. Han, Y. Hou, W. Bao, C. Zhang, G. Feng, L. Chang, Z. Huang and J. Wang, Improved Activity and SO<sub>2</sub> Resistance by Sm-Modulated Redox of MnCeSmTiO<sub>x</sub> Mesoporous Amorphous Oxides for Low-Temperature NH<sub>3</sub>-SCR of NO, *ACS Catal.*, 2020, **10**(16), 9034–9045.
  - 31 D. Meng, W. Zhan, Y. Guo, Y. Guo, L. Wang and G. Lu, A Highly Effective Catalyst of Sm-MnO<sub>x</sub> for the NH<sub>3</sub>-SCR of NO<sub>x</sub> at Low Temperature: Promotional Role of Sm and Its Catalytic Performance, *ACS Catal.*, 2015, **5**(10), 5973–5983.
  - 32 L. E. Gevers, L. R. Enakonda, A. Shahid, S. Ould-Chikh, C. I. Q. Silva, P. P. Paalanen, A. Aguilar-Tapia, J.-L. Hazemann, M. N. Hedhili, F. Wen and J. Ruiz-Martínez, Unraveling the structure and role of Mn and Ce for NO<sub>x</sub> reduction in application-relevant catalysts, *Nat. Commun.*, 2022, **13**(1), 2960.
  - 33 L. Zhang, L. Li, Y. Cao, X. Yao, C. Ge, F. Gao, Y. Deng, C. Tang and L. Dong, Getting insight into the influence of SO<sub>2</sub> on TiO<sub>2</sub>/CeO<sub>2</sub> for the selective catalytic reduction of NO by NH<sub>3</sub>, *Appl. Catal., B*, 2015, **165**, 589–598.
  - 34 M. Waqif, P. Bazin, O. Saur, J. C. Lavalley, G. Blanchard and O. Touret, Study of ceria sulfation, *Appl. Catal., B*, 1997, **11**(2), 193–205.
  - 35 J. Li, C. Zhang, Q. Li, T. Gao, S. Yu, P. Tan, Q. Fang and G. Chen, Promoting mechanism of SO<sub>2</sub> resistance performance by anatase TiO<sub>2</sub> {001} facets on Mn-Ce/TiO<sub>2</sub> catalysts during NH<sub>3</sub>-SCR reaction, *Chem. Eng. Sci.*, 2022, **251**, 117438.
  - 36 M. C. Biesinger, B. P. Payne, A. P. Grosvenor, L. W. M. Lau, A. R. Gerson and R. S. C. Smart, Resolving surface chemical states in XPS analysis of first row transition metals, oxides and hydroxides: Cr, Mn, Fe, Co and Ni, *Appl. Surf. Sci.*, 2011, **257**(7), 2717–2730.
  - 37 R. M. Ferrizz, R. J. Gorte and J. M. Vohs, TPD and XPS Investigation of the Interaction of SO<sub>2</sub> with Model Ceria Catalysts, *Catal. Lett.*, 2002, **82**(1), 123–129.



- 38 B. Jiang, B. Deng, Z. Zhang, Z. Wu, X. Tang, S. Yao and H. Lu, Effect of Zr Addition on the Low-Temperature SCR Activity and SO<sub>2</sub> Tolerance of Fe-Mn/Ti Catalysts, *J. Phys. Chem. C*, 2014, **118**(27), 14866–14875.
- 39 J. Liu, R.-T. Guo, M.-Y. Li, P. Sun, S.-M. Liu, W.-G. Pan, S.-W. Liu and X. Sun, Enhancement of the SO<sub>2</sub> resistance of Mn/TiO<sub>2</sub> SCR catalyst by Eu modification: A mechanism study, *Fuel*, 2018, **223**, 385–393.
- 40 M. Koebel, M. Elsener and G. Madia, Reaction Pathways in the Selective Catalytic Reduction Process with NO and NO<sub>2</sub> at Low Temperatures, *Ind. Eng. Chem. Res.*, 2001, **40**(1), 52–59.
- 41 G. Madia, M. Koebel, M. Elsener and A. Wokaun, The Effect of an Oxidation Precatalyst on the NO<sub>x</sub> Reduction by Ammonia SCR, *Ind. Eng. Chem. Res.*, 2002, **41**(15), 3512–3517.
- 42 F. Lin, Y. He, Z. Wang, Q. Ma, R. Whiddon, Y. Zhu and J. Liu, Catalytic oxidation of NO by O<sub>2</sub> over CeO<sub>2</sub>-MnO<sub>x</sub>: SO<sub>2</sub> poisoning mechanism, *RSC Adv.*, 2016, **6**(37), 31422–31430.
- 43 N. Tang, Y. Liu, H. Wang and Z. Wu, Mechanism Study of NO Catalytic Oxidation over MnO<sub>x</sub>/TiO<sub>2</sub> Catalysts, *J. Phys. Chem. C*, 2011, **115**(16), 8214–8220.
- 44 F. Arena, T. Torre, C. Raimondo and A. Parmaliana, Structure and redox properties of bulk and supported manganese oxide catalysts, *Phys. Chem. Chem. Phys.*, 2001, **3**(10), 1911–1917.
- 45 X. Wu, Q. Liang, D. Weng, J. Fan and R. Ran, Synthesis of CeO<sub>2</sub>-MnO<sub>x</sub> mixed oxides and catalytic performance under oxygen-rich condition, *Catal. Today*, 2007, **126**(3), 430–435.
- 46 S. Yang, Y. Guo, H. Chang, L. Ma, Y. Peng, Z. Qu, N. Yan, C. Wang and J. Li, Novel effect of SO<sub>2</sub> on the SCR reaction over CeO<sub>2</sub>: Mechanism and significance, *Appl. Catal., B*, 2013, **136-137**, 19–28.
- 47 D. W. Kwon, K. H. Park and S. C. Hong, Enhancement of SCR activity and SO<sub>2</sub> resistance on VO<sub>x</sub>/TiO<sub>2</sub> catalyst by addition of molybdenum, *Chem. Eng. J.*, 2016, **284**, 315–324.

